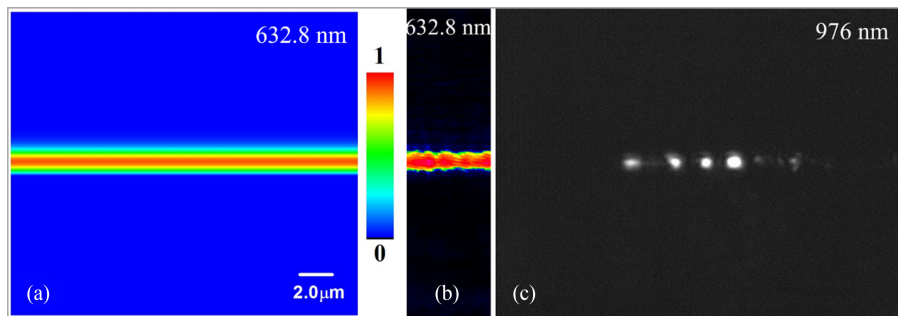


Optical Ridge Waveguides in Magneto-Optical Glasses Fabricated by Combination of Silicon Ion Implantation and Femtosecond Laser Ablation

Volume 10, Number 5, September 2018

Qi-Feng Zhu
Yue Wang
Xiao-Liang Shen
Hai-Tao Guo
Chun-Xiao Liu



DOI: 10.1109/JPHOT.2018.2867491
1943-0655 © 2018 IEEE

Optical Ridge Waveguides in Magneto-Optical Glasses Fabricated by Combination of Silicon Ion Implantation and Femtosecond Laser Ablation

Qi-Feng Zhu,¹ Yue Wang,¹ Xiao-Liang Shen,¹ Hai-Tao Guo,² and Chun-Xiao Liu¹ 

¹College of Electronic and Optical Engineering, Nanjing University of Posts and Telecommunications, Nanjing 210023, China

²State Key Laboratory of Transient Optics and Photonics, Xi'an Institute of Optics and Precision Mechanics, Chinese Academy of Sciences (CAS), Xi'an 710119, China

DOI:10.1109/JPHOT.2018.2867491

1943-0655 © 2018 IEEE. Translations and content mining are permitted for academic research only.
Personal use is also permitted, but republication/redistribution requires IEEE permission. See
http://www.ieee.org/publications_standards/publications/rights/index.html for more information.

Manuscript received August 10, 2018; revised August 21, 2018; accepted August 23, 2018. Date of publication August 28, 2018; date of current version September 13, 2018. This work was supported in part by the Postgraduate Research and Practice Innovation Program of Jiangsu Province under Grant SJCX18_0292, and in part by the National Natural Science Foundation of China under Grants 11405041, 51502144 and 61475189. Corresponding author: Chun-Xiao Liu (e-mail: cxliu0816@sina.com).

Abstract: Tb³⁺-doped aluminum borosilicate glass is a promising magneto-optical material that can be used to fabricate Faraday rotating devices. In this paper, we report the fabrication of an optical ridge waveguide structure in the Tb³⁺-doped aluminum borosilicate glass by using a combination of femtosecond laser ablation and ion implantation. The end-face microscopic photographs of the waveguide were acquired by the optical microscope. The effective refractive indices of the modes and near-field intensity distributions were measured by the prism-coupling and end-face coupling techniques. The distributions of energy loss, refractive index, and light intensity were simulated by the stopping and range of ions in matter 2013, reflectivity calculation method, and finite-difference beam propagation method. The results provide a new idea for the fabrication of waveguide-type magneto-optical isolators.

Index Terms: Optical ridge waveguide, ion implantation, femtosecond laser ablation.

1. Introduction

The reverse propagation light in the optical circuit has a negative effect on the light source and the optical system. An optical isolator is a passive optical device that only allows light to pass in one direction. Its function is to prevent the reverse propagation light caused by various reasons, thereby improving the efficiency of the light propagation. With the further development of optical communication technology, people have also put forward higher requirements for optical isolator performance indicators including integration and functionalization. Therefore, the study of a new generation of optical isolator has become the need for optical communication system. On the other hand, the optical waveguide is a basic unit of integrated optics. Therefore, the waveguide isolator that combines the properties of an isolator and an optical waveguide has gradually become a research hotspot. An optical waveguide structure fabricated in a Faraday magneto-optical material is the basis of achieving the waveguide isolator [1]–[9].

There are many fabrication methods for optical waveguides, such as ion implantation/irradiation, ion exchange, metal ion diffusion, femtosecond laser inscription [10]–[14] and so on. As a mature material modification technique, ion implantation is widely applied in the formation of optical planar waveguides [15], [16]. In addition, compared with a planar (one dimension) waveguide, a ridge waveguide (two dimensions) can limit the propagation of light in two dimensions and is easier to couple with an optical fiber [17]. The applications of the ridge waveguide are more widely in the integrated optical circuits [18]. Therefore, ion implantation must be combined with other techniques, such as diamond blade dicing, wet etching, laser ablation and so on, to construct a ridge waveguide structure [19]. The femtosecond laser ablation is a competitive technique because it has a very short pulse and can quickly ablate a specific portion on the surface of the sample [20]–[23]. Compared with the more commonly used method (such as lithography), no mask is necessary for the preparation process. Therefore, the combination of ion implantation/irradiation and femtosecond (fs) laser ablation technique has become a popular technique to fabricate ridge waveguide structures [24].

Magneto-optical glass is an optical functional material newly developed in recent decades. Due to its own Faraday effect, it has been widely used in optical isolators, circulators and other magneto-optical devices [25], [26]. Compared with magneto-optical crystals including $\text{Y}_3\text{Fe}_5\text{O}_{12}$ and $\text{Gd}_2\text{BiFe}_3\text{O}_{12}$, the magneto-optical glasses have superior magneto-optical performances, simple preparation, low cost, and easy formation of large size [27], [28]. Therefore, the development prospect of the magneto-optical glass will be broad in the future. In the present experiments, the Tb^{3+} -doped aluminum borosilicate glass ($\text{Tb}_2\text{O}_3\text{-SiO}_2\text{-Al}_2\text{O}_3\text{-B}_2\text{O}_3$) was applied to fabricate an optical ridge waveguide structure. In magneto-optical materials, the Verdet constant is an important parameter. The Verdet constant of the Tb^{3+} -doped aluminum borosilicate glass is -0.33 min/Oe/cm at a wavelength of 632.8 nm [29]. Because of its non-magnetic saturation, high transmittance, low nonlinear index, good material uniformity and high Verdet constant, the Tb^{3+} -doped aluminum borosilicate glass can be used as a material for fabricating optical ridge waveguide.

In this work, we report on the fabrication of a ridge waveguide in the magneto-optical glass by combining ion implantation and femtosecond laser ablation for the first time to our knowledge. The characteristics of the waveguide have been measured and discussed in detail.

2. Experiments

The Tb^{3+} -doped aluminum borosilicate glass was prepared by the traditional melt-quenching method. The composition of the magneto-optical glass is $\text{SiO}_2\text{-B}_2\text{O}_3\text{-Al}_2\text{O}_3\text{-Tb}_2\text{O}_3$. The size of the experimental sample is $10.0 \text{ mm} \times 10.0 \text{ mm} \times 1.0 \text{ mm}$. In order to reduce the scattering loss that is due to the unevenness of the surface, the sample was optically polished before the waveguide fabrication. And the refractive index of the Tb^{3+} -doped aluminum borosilicate glass was measured by using the prism coupling method before the ion implantation.

There are two steps to fabricate an optical ridge waveguide. Firstly, the polished surface ($10 \text{ mm} \times 10 \text{ mm}$) of the sample was implanted with Si ions having an energy of 6.0 MeV and a dose of $2.0 \times 10^{15} \text{ ions/cm}^2$ at room temperature. The energy was chosen based on the desired thickness of the magneto-optical glass waveguide and the fluence was selected in consideration of the damage ratio. The ion implantation process is shown in Fig. 1(a). To avoid the channel effect, the normal direction of the glass surface was at an angle of 7° to the direction of the incident ion beam during the ion implantation process. The ion current density was limited to 50 nA/cm^2 to prevent the thermal effect. The ion implantation was performed on a $2 \times 1.7 \text{ MV}$ tandem accelerator at Peking University. After the ion implantation, a planar optical waveguide structure was fabricated on the Tb^{3+} -doped aluminum borosilicate glass surface. Secondly, in order to fabricate a ridge waveguide, we utilized a Ti: Sapphire laser system with a repetition rate of 1 kHz, which delivered 220 fs pulses and linearly polarized at 800 nm, to ablate the previous ion-implanted surface. Fig. 1(b) shows the process of the ridge waveguide fabrication. The sample was placed at a three-dimensional adjustment platform with a spatial resolution of $0.2 \mu\text{m}$. The femtosecond laser was focused on the surface of the sample through a $20 \times$ microscope objective (N.A. = 0.4) and ablated at a

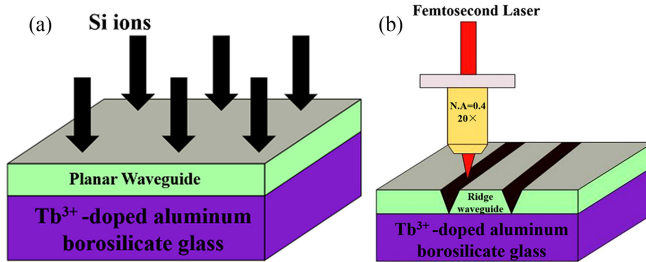


Fig. 1. Schematic for the (a) planar and (b) ridge waveguide fabrication in the Tb³⁺-doped aluminum borosilicate glass.

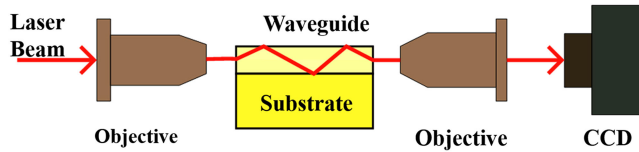


Fig. 2. Schematic for the end-face coupling measurement.

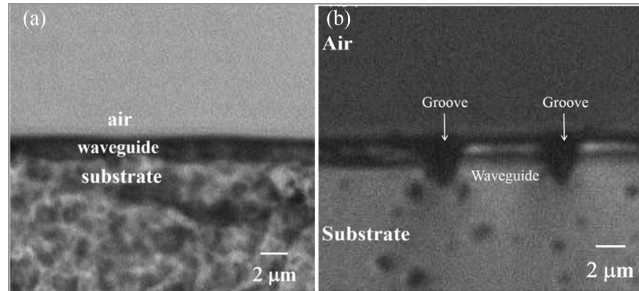


Fig. 3. Optical microscope images of (a) the planar waveguide and (b) the ridge waveguide in the Tb³⁺-doped aluminum borosilicate glass.

scanning speed of 200 $\mu\text{m}/\text{s}$. After the femtosecond laser ablation, a ridge structure was fabricated on the planar optical waveguide. Then, for the purpose of improving the optical qualities (such as propagation properties) of the waveguide, the sample was annealed at 260 °C for 60 min in air. It was because that 260 °C was within the moderate annealing temperature range (200–400 °C) and smaller than the Tg (transition temperature) of the magneto-optical glass.

After the ridge waveguide was fabricated, we characterized the properties of the waveguide. In order to study the layer area distribution of the waveguide, we used an optical microscope to observe the end face of the waveguide. The dark-mode spectrum of the waveguide at a wavelength of 632.8 nm was measured by a Model 2010 Prism Coupler. The near-field intensity distribution of the waveguide was captured by the end-face coupling device. Fig. 2 shows the schematic diagram of the end-face coupling device. The light from the He-Ne laser/semiconductor laser was coupled into the waveguide through the first $\times 25$ microscope objective lens. And then the light transmitted from the waveguide was imaged onto a CCD camera through the second $\times 25$ microscope objective lens. The two lenses and waveguide were installed on three-dimensional translation stages, respectively.

3. Results and Discussion

Fig. 3(a) shows the end-face microscopic photograph of the silicon-implanted Tb³⁺-doped aluminum borosilicate glass, which was acquired by the optical microscope. Obviously, three distinct layers can be seen in the microscope image, where the middle is the planar waveguide formed by the

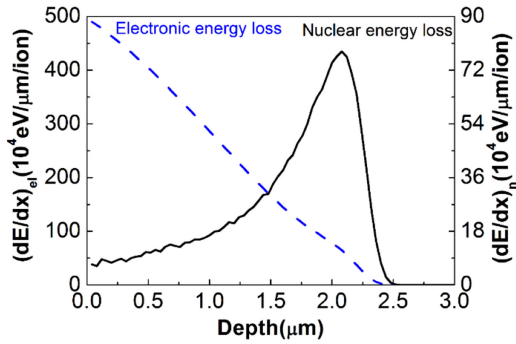


Fig. 4. Electronic and nuclear energy losses of the implanted silicon ions in the Tb^{3+} -doped aluminum borosilicate glass.

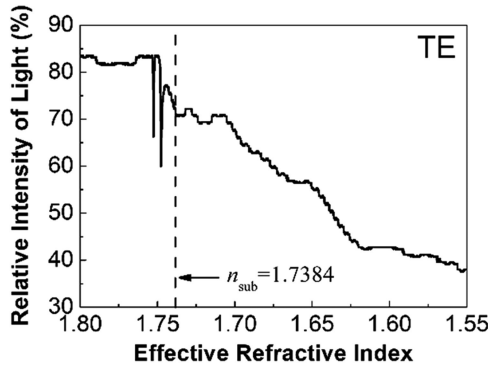


Fig. 5. Effective refractive indices of the modes for the implanted Tb^{3+} -doped aluminum borosilicate glass.

ion implantation. The thickness of the waveguide layer is about $2.1 \mu\text{m}$. Fig. 3(b) exhibits the microscope image of the ridge waveguide. It can be seen that an optical ridge waveguide with a width of $7.1 \mu\text{m}$ is produced on the planar waveguide after the fs laser ablation. In addition, the sidewalls of the ridge waveguide are relatively smooth and the roughness is estimated to be $0.5 \mu\text{m}$.

In order to explore the implantation depth and the energy losses of the 6.0 MeV Si ions in the Tb^{3+} -doped aluminum borosilicate glass, we simulated the ion implantation process by using the Stopping and Range of Ions in Matter (SRIM) 2013 code [30], as shown in Fig. 4. From the figure we can see, in the range of $0 \sim 1.5 \mu\text{m}$, the main loss of the Si ion implantation is the electronic energy loss and the peak value is 5.00 keV/nm on the surface of the sample. However, in the range of $1.5 \sim 2.5 \mu\text{m}$, the nuclear energy loss is dominant and the maximum value reaches 0.77 keV/nm at the depth of $2.08 \mu\text{m}$, which is in agreement with the waveguide thickness in Fig. 3(a). It suggests that an optical barrier is formed at the end of the ion range due to the nuclear energy loss.

Fig. 5 shows the dark-mode spectrum of the silicate-implanted Tb^{3+} -doped aluminum borosilicate glass waveguide by the prism coupling method. There are two modes excited in the waveguide and their effective refractive indices are 1.7525 and 1.7477 at 632.8 nm . The dotted line in the Fig. 5 illustrates that the substrate refractive index of the glass is 1.7384 . By comparing the refractive indices of the modes and the substrate, we can find that the effective refractive index of the each waveguide mode is higher than that of the substrate. It indicates that ion implantation forms a waveguide structure with an increased refractive index.

Because the refractive index distribution of a waveguide is more difficult to be measured directly by experiments, so we used the reflectivity calculation method (RCM) [31] to reconstruct the refractive index profile. The RCM is a technique that is proposed by Chandler and Lama to simulate the

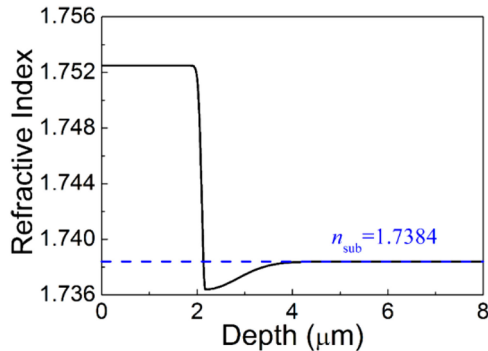


Fig. 6. The refractive index distribution of the Tb^{3+} -doped aluminum borosilicate glass waveguide reconstructed by the RCM.

TABLE 1
The Effective Refractive Indices of the Measured and Calculated Modes for the Silicon-Implanted Tb^{3+} -Doped Aluminum Borosilicate Glass Waveguide

Mode order	Effective refractive index		
	Exp.	Cal.	Difference
0	1.7525	1.7483	4.2×10^{-3}
1	1.7475	1.7376	9.9×10^{-3}
2	1.7377	1.7347	3.0×10^{-3}

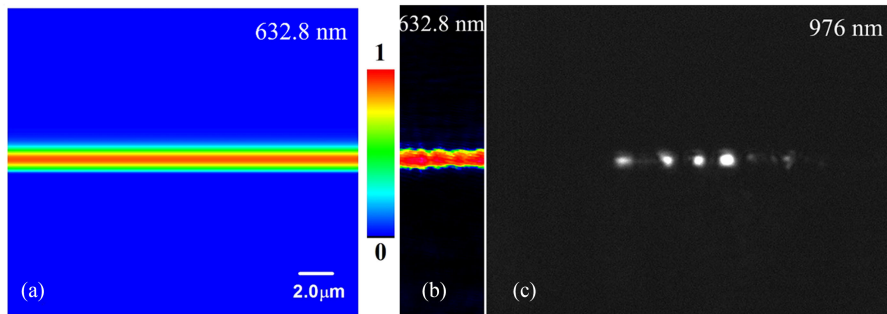


Fig. 7. (a) Simulated and (b) measured near-field intensity distributions of the modes in the planar waveguide, and (c) measured mode intensity distribution at 976 nm in the ridge waveguide.

refractive index distribution of a waveguide, as shown in Fig. 6. From the figure we can see, the refractive index increases by about 0.8% in the region of 0 to 2.0 μm and reduces by about 0.13% at the end of the ion implantation track. It means a refractive index increasing-type waveguide structure is formed owing to the ion implantation. The refractive index distribution of the waveguide is a typical “well” + “barrier” type. Table 1 lists the effective refractive indices of the measured and calculated modes. As we can see, the differences between the experimental and the calculated values are on the order of 10^{-3} , which indicates that the simulation of the RCM is better.

Fig. 7(a) depicts the light intensity distribution of the TE_0 mode simulated by the finite-difference beam propagation method (FD-BPM), which is based on the refractive index distribution of the waveguide [32]. Obviously, the width in the vertical direction is approximately 2.0 μm , which is the same as the thickness of the waveguide layer in Fig. 3(a). Fig. 7(b) shows the near-field intensity distribution of the TE_0 mode by using the end-face coupling method. It can be seen from the figure

that the silicon-implanted Tb^{3+} -doped aluminum borosilicate glass waveguide can better confine the propagation of light. The distribution of the light intensity is uneven in the figure, which is mainly due to the poor polishing. By comparing Fig. 7(a) with Fig. 7(b), we can see that the calculated intensity distribution is in agreement with the measured one, which shows that the near-field light intensity distribution based on the refractive index distribution of the waveguide is reasonable. Fig. 7(c) shows the near-field intensity distribution of the ridge waveguide at 976 nm measured by the end-face coupling method. The measured mode profile suggests that the distribution of the near-field intensity is consistent with the structure of the ridge waveguide in Fig. 3(b). Propagation loss is a pretty important parameter for a waveguide and measured by the end-face coupling technique in the work. The propagation losses in the planar and ridge waveguides are estimated to be 2.3 dB/cm and 3.4 dB/cm, respectively. It can be seen that the side wall roughness induced by the femtosecond laser ablation resulted in additional scattering loss for the ridge waveguide.

4. Conclusion

In conclusion, a ridge waveguide in the Tb^{3+} -doped aluminum borosilicate glass has been fabricated by using a combination of femtosecond laser ablation and ion implantation. The end-face microscopic photograph of the waveguide shows that the thickness of the waveguide layer is about $2.1\ \mu m$. The simulation of the RCM suggests that the refractive index distribution of the waveguide is a typical “well” + “barrier” type. The near-field intensity distribution of the TE_0 mode at 632.8 nm indicates that the waveguide can better confine the propagation of light. The measured mode intensity distribution at 976 nm in the ridge waveguide suggests that the light propagation could be remarkably confined in two dimensions. The research has important value for fabricating waveguide-type magneto-optical isolator.

References

- [1] K. N. Jarvis, J. A. Devlin, T. E. Wall, B. E. Sauer, and M. R. Tarbutt, “Blue-detuned magneto-optical trap,” *Phys. Rev. Lett.*, vol. 120, 2018, Art. no. 083201.
- [2] L. D. Tzuang, K. J. Fang, P. Nussenzveig, S. H. Fan, and M. Lipson, “Non-reciprocal phase shift induced by an effective magnetic flux for light,” *Nature Photon.*, vol. 8, no. 9, pp. 701–705, 2014.
- [3] P. Wang *et al.*, “Insights into magneto-optics of helical conjugated polymers,” *J. Amer. Chem. Soc.*, vol. 140, no. 20, pp. 6501–6508, 2018.
- [4] L. Zhang, D. X. Yang, K. Chen, T. Li, and S. Xia, “Design of nonreciprocal waveguide devices based on two-dimensional magneto-optical photonic crystals,” *Opt. Laser Technol.*, vol. 50, pp. 195–201, 2013.
- [5] C. Ríos *et al.*, “Integrated all-photonic nonvolatile multilevel memory,” *Nature Photon.*, vol. 9, no. 11, pp. 725–732, 2015.
- [6] X. H. Li *et al.*, “High-power graphene mode-locked Tm/Ho co-doped fiber laser with evanescent field interaction,” *Sci. Rep.*, vol. 5, 2015, Art. no. 16624.
- [7] G. C. Shan, C. H. Shek, and M. J. Hu, “Developments of cavity-controlled devices with graphene and graphene nanoribbon for optoelectronics applications,” in *Graphene Science Handbook*. Boca Raton, FL, USA: CRC Press, 2016, pp. 395–410.
- [8] X. H. Li *et al.*, “All-fiber dissipative solitons evolution in a compact passively Yb-doped mode-locked fiber laser,” *J. Lightw. Technol.*, vol. 30, no. 15, pp. 2502–2507, Aug. 2012.
- [9] X. H. Li *et al.*, “Broadband saturable absorption of graphene oxide thin film and its application in pulsed fiber lasers,” *IEEE J. Sel. Topics Quantum Electron.*, vol. 20, no. 5, pp. 441–447, Sep./Oct. 2014.
- [10] Y. Jiang *et al.*, “Model of refractive-index changes in lithium niobate waveguides fabricated by ion implantation,” *Phys. Rev. B*, vol. 75, 2007, Art. no. 195101.
- [11] F. Chen, “Micro- and submicrometric waveguiding structures in optical crystals produced by ion beams for photonic applications,” *Laser Photon. Rev.*, vol. 6, no. 5, pp. 622–640, 2012.
- [12] A. Tervonen, B. R. West, and S. Honkanen, “Ion-exchanged glass waveguide technology: A review,” *Opt. Eng.*, vol. 50, no. 7, 2011, Art. no. 071107.
- [13] H. Hu, R. Ricken, and W. Sohler, “Low-loss ridge waveguides on lithium niobate fabricated by local diffusion doping with titanium,” *Appl. Phys. B*, vol. 98, no. 4, pp. 677–679, 2010.
- [14] Y. Tan, J. R. Vázquez de Aldana, and F. Chen, “Femtosecond laser written lithium niobate waveguide laser operating at 1085 nm,” *Opt. Eng.*, vol. 53, no. 10, 2014, Art. no. 107109.
- [15] I. Bányaśz, Z. Zolnai, M. Fried, S. Berneschi, S. Pelli, and G. Nunzi-Conti, “Leaky mode suppression in planar optical waveguides written in $Er:TeO_2-WO_3$ glass and CaF_2 crystal via double energy implantation with MeV N^+ ions,” *Nucl. Instrum. Methods Phys. Res. Section B, Beam Interact. Mater. Atoms*, vol. 326, pp. 81–85, 2014.

- [16] Y. Tan, C. Zhang, F. Chen, F. Q. Liu, D. Jaque, and Q. M. Lu, "Room-temperature continuous wave laser oscillations in Nd:YAG ceramic waveguides produced by carbon ion implantation," *Appl. Phys. B*, vol. 103, no. 4, pp. 837–840, 2011.
- [17] G. V. Vázquez, R. Vallente, S. Gómez-Salces, E. Flores-Romero, J. Rickards, and R. Trejo-Luna, "Carbon implanted waveguides in soda lime glass doped with Yb^{3+} and Er^{3+} for visible light emission," *Opt. Laser Technol.*, vol. 79, pp. 132–136, 2016.
- [18] D. Kip, "Photorefractive waveguides in oxide crystals: Fabrication, properties, and applications," *Appl. Phys. B*, vol. 67, no. 2, pp. 131–150, 1998.
- [19] J. D. B. Bradley and M. Pollnau, "Erbium-doped integrated waveguide amplifiers and lasers," *Laser Photon. Rev.*, vol. 5, no. 3, pp. 368–403, 2011.
- [20] S. Juodkazis, V. Mizeikis, and H. Misawa, "Three-dimensional microfabrication of materials by femtosecond lasers for photonics applications," *J. Appl. Phys.*, vol. 106, no. 5, 2009, Art. no. 051101.
- [21] K. Sugiyama and Y. Cheng, "Ultrafast lasers—reliable tools for advanced materials processing," *Light: Sci. Appl.*, vol. 3, 2014, Art. no. 149.
- [22] Y. C. Jia, E. R. Rüter, S. Akhmadaliev, S. Q. Zhou, F. Chen, and D. Kip, "Ridge waveguide lasers in Nd:YAG crystals produced by combining swift heavy ion irradiation and precise diamond blade dicing," *Opt. Mater. Exp.*, vol. 3, no. 4, pp. 433–438, 2013.
- [23] H. Shin and D. Kim, "Cutting thin glass by femtosecond laser ablation," *Opt. Laser Technol.*, vol. 102, pp. 1–11, 2018.
- [24] A. B. Yashar, H. Ilan, and A. J. Agranat, "Construction of waveguiding structures in potassium lithium tantalate niobate crystals by combined laser ablation and ion implantation," *Appl. Phys. A*, vol. 118, no. 2, pp. 403–407, 2015.
- [25] C. B. Pedroso, E. Munin, A. B. Villaverde, N. Aranha, V. C. Solano Reynoso, and L. C. Barbosa, "Magneto-optical rotation of heavy-metal oxide glasses," *J. Non-Crystalline Solids*, vol. 231, no. 1/2, pp. 134–142, 1998.
- [26] W. N. Li, K. S. Zou, M. Lu, B. Peng, and W. Zhao, "Faraday glasses with a large size and high performance," *Int. J. Appl. Ceram. Technol.*, vol. 7, no. 3, pp. 369–374, 2010.
- [27] J. X. Ding *et al.*, "Influence of Tb^{3+} concentration on the optical properties and Verdet constant of magneto-optic ABS-PZZ glass," *Opt. Mater.*, vol. 69, pp. 202–206, 2017.
- [28] M. Valeanu *et al.*, "The relationship between magnetism and magneto-optical effects in rare earth doped aluminophosphate glasses," *J. Phys. D, Appl. Phys.*, vol. 49, no. 7, 2016, Art. no. 075001.
- [29] C. X. Liu *et al.*, "Optical waveguides in magneto-optical glasses fabricated by proton implantation," *Opt. Laser Technol.*, vol. 85, pp. 55–59, 2016.
- [30] J. F. Ziegler, SRIM—The stopping and range of ions in matter. 2013. [Online]. Available: <http://www.srim.org>
- [31] P. J. Chandler and F. L. Lama, "A new approach to the determination of planar waveguide profiles by means of a nonstationary mode index calculation," *Optica Acta Int. J. Opt.*, vol. 33, no. 2, pp. 127–143, 1986.
- [32] Rsoft Design Group, Computer software BeamPROP version8.0. 2016. [Online]. Available: <http://www.rsoftdesign.com>